

# Chiral-induced spin selectivity augments quantum coherence in avian compass

Yash Tiwari and Vishvendra Singh Poonia\*

*Department of Electronics and Communication, Indian Institute of Technology, Roorkee, India*

(Dated: December 9, 2022)

This work investigates the effect of chiral-induced spin selectivity (CISS) on quantum spin coherence in the radical pair mechanism of avian magnetoreception. Additionally, we examine the utilitarian role of coherence for the avian compass by analyzing its correlation with the yield of the signaling state. We find that both the relative entropy of global coherence and local coherence in the radical pair increases with CISS. However only the global coherence exhibit the utilitarian role for the avian compass. We also analyze the interplay of dipolar interaction with the CISS and their effect on coherence of the radical pair. Further, we analyze the effect of environmental decoherence along with CISS. We conclude that a high CISS results in a high correlation of global coherence with signaling state yield. It confirms that CISS plays an important role both for compass sensitivity and coherence in the avian compass.

## I. INTRODUCTION

Coherence is a resource for quantum technologies, and its existence and utility for the biological processes occurring at ambient conditions have been extremely intriguing. Avian magnetoreception is one such biological process where the radical pair spin dynamics, along with the role and utility of quantum coherence, has been investigated from several aspects [1–8]. The radical pair mechanism is based on a spin-sensitive chemical reaction that is mediated by a protein molecule [9–11]. Owing to the chirality of protein molecules, the chiral-induced spin selectivity (CISS) effect could play an essential role in the electron transport part of the reaction. The origin of CISS is attributed to the spin-orbit interaction and the electrostatic potential provided by the chiral molecules [12–19]. It was shown by Fay et al. [20] that chirality in conjunction with spin-orbit reaction in electron transfer reaction generates coherence locally. It was done for the electron spin echo experiment. It was also shown in [21] that the prerequisite for forming a radical pair for avian magneto-reception is the transfer of electrons. This transfer or transport of electrons between donor and acceptor occurs in a chiral molecule contributing toward CISS and affecting the operation of the avian compass.

Coherence quantifiers are based on the non-diagonal/coherence element of the density matrix of a quantum state [22–24]. It has been suggested in references [1, 25] that global coherence rather than local or electronic coherence might enhance the compass sensitivity. Therefore, we correlate the yield of the spin-selective chemical reaction with coherence in a chiral medium for the avian-magnetoreception.

In this work, we make use of relative entropy of coherence [22] and total coherence [3] as coherence quantifiers to answer the following questions: i) how does the CISS affect the local and global coherence in avian compass, ii)

how do dipolar and exchange interaction in conjunction with CISS affect the total local and global coherence measures, iii) how does the environmental decoherence affect the multi-nuclei radical pair mechanism, and more importantly iv) does the quantum coherence play any utilitarian role for the avian compass? If yes, in what form? We have considered the case of three nuclei each on flavin adenine dinucleotide FAD and tryptophan TrpH radicals. The FAD act as a donor entity, whereas TrpH act as an acceptor entity. The hyperfine interaction values of these nuclei have been taken from ref. [9].

The manuscript has been organized as follows: Section II discusses the methodology followed for analysis. Section III discusses the results, wherein subsection III A discusses the effect of CISS on quantum coherence, and subsection III B explores the impact of electron-electron interactions on system sensitivity along with CISS. Section III C illustrate an increase of coherence due to CISS at various rate combinations. Section IV demonstrates the effect of environmental decoherence on the system. Section V examines the utilitarian aspect of the quantum coherence in the avian compass.

## II. METHODOLOGY

In the radical pair model of the avian compass, an electron is photo-excited in the acceptor molecule, creating a vacancy in the ground state. Another electron from a neighboring donor molecule travels in the chiral medium to fill this vacancy. It results in the formation of a radical pair where the spin state of the electron on the donor molecule is  $\hat{S}_D$  and on the acceptor molecule is  $\hat{S}_A$  [21, 26].

The spin state of the above formed radical is governed by Hamiltonian given by [21, 27, 28]

$$\hat{H} = \omega \cdot (\hat{S}_A + \hat{S}_D) + \sum_{i \in D, A} \sum_k \hat{S}_i \cdot A_{ik} \cdot \hat{I}_{ik} - J(2\hat{S}_A \cdot \hat{S}_D + 0.5) + \hat{S}_A \cdot D \cdot \hat{S}_B \quad (1)$$

where  $\omega = g\bar{\mu}_B \bar{B}$ ,  $\bar{B} =$

\* vishvendra@ece.iit.ac.in

$B_0((\cos\theta\cos\phi)\bar{x} + (\cos\theta\sin\phi)\bar{y} + (\cos\theta)\bar{z})$ .  $B_0$  corresponds to the earth's magnetic field.  $\theta$  and  $\phi$  correspond to the orientation of the magnetic field with respect to hyperfine tensor [4].  $J$  and  $D$  are the exchange and dipolar interactions.  $A$  is the hyperfine tensor depicting interactions between electrons and neighboring nuclear spins.

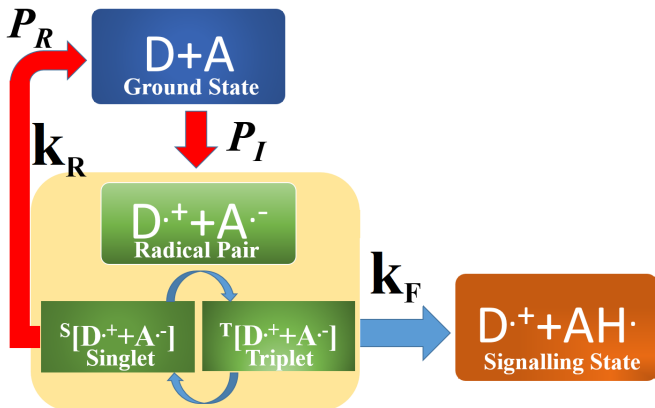


FIG. 1. The schematic for the CISS-assisted radical pair mechanism where  $D$  denotes the donor molecule,  $A$  represents the acceptor molecule.  $D^+$  is the donor radical,  $A^-$  is the acceptor radical,  $k_F$  is the protonation rate to the signalling state and  $k_R$  is the recombination rate (back to the ground state). The red arrows represent the role of CISS in the reaction pathways.

The spin state of the radical pair evolves under Zeeman and hyperfine interactions. Along with this evolution of the spin state, the radical pair also recombines back as shown in Fig. 1. The recombination either happens back to the ground state or to the signaling state (via protonation with  $H^+$  of the acceptor radical, cf. Fig. 1). The CISS plays role in the formation and recombination of the radical pair as they involve electron transport through the chiral medium. Therefore, the effect of CISS is captured by the initial state  $P_I$  and recombination state  $P_R$ , also shown with red arrows in Fig. 1. The signaling state does not involve the transfer of electrons (only  $H^+$  involved), therefore, CISS is not involved in its formation (shown with the blue arrow in Fig. 1). We define [21]:

$$|\psi_I\rangle = \frac{1}{\sqrt{2}}[\sin(0.5\chi) + \cos(0.5\chi)]|\uparrow_D\downarrow_A\rangle + \frac{1}{\sqrt{2}}[\sin(0.5\chi) - \cos(0.5\chi)]|\downarrow_D\uparrow_A\rangle \quad (2)$$

Then the initial density matrix is given as:  $P_I = |\psi_I\rangle\langle\psi_I| \otimes \frac{I}{Z}$ , where  $\frac{I}{Z}$  corresponds to the mixed state of nuclei, and  $Z$  is size of the Hilbert space of the nuclei. The recombination operator  $P_R = |\psi_R\rangle\langle\psi_R|$  accounts for

recombination to the ground state where  $|\psi_R\rangle$  is:

$$|\psi_R\rangle = -\frac{1}{\sqrt{2}}[\sin(0.5\chi) - \cos(0.5\chi)]|\uparrow_D\downarrow_A\rangle - \frac{1}{\sqrt{2}}[\sin(0.5\chi) + \cos(0.5\chi)]|\downarrow_D\uparrow_A\rangle \quad (3)$$

The CISS parameter  $\chi \in [0, \frac{\pi}{2}]$  depends on the spin selectivity of the reactants medium;  $\chi = 0$  corresponding to no CISS and  $\chi = \pi/2$  corresponding to the maximum CISS. The master equation governing the state evolution of the system is given as:

$$\frac{d\hat{\rho}}{dt} = -i[\hat{H}, \hat{\rho}(t)] - \frac{1}{2}k_R[P_R, \hat{\rho}(t)] - k_F\hat{\rho}(t) \quad (4)$$

Where  $k_F$  is the protonation rate to the signalling state, and  $k_R$  is the recombination rate (back to the ground state) [21, 26].

### III. RESULTS

This section is divided into three subsections. In the first subsection, we analyze the effect of CISS on the local and global coherence in the radical pair system. Interestingly, we observe that the CISS enhances both local and global coherences in the radical pair system. In the second subsection, we examine the effect of the dipolar interactions on global and local coherence along with CISS in the RP model. In the last subsection, we study the coherence in RP system as a function of recombination and protonation rates ( $k_R$  and  $k_F$ ).

#### A. Effect of CISS on Coherence

To quantify the coherence in the radical pair system, we use the von-Neumann entropy  $S(\rho)$ , which is given in Eq. 5 where  $Tr$  corresponds to the trace of a matrix. It has a minimum value of zero for pure states and a maximum value of  $\ln(d)$ , where  $d$  is the dimension of the Hilbert space of the system. The maximum value corresponds to the maximally mixed state of the system.

$$S(\rho) = -Tr(\rho \ln(\rho)) \quad (5)$$

With the von-Neumann entropy, the coherence quantifier of the RP system can be defined by the relative entropy of local and global coherence, as given in Eq. 6 and Eq. 7 respectively [22].

$$C_L(\rho) = S(\rho_{diag}^{el}) - S(\rho^{el}) \quad (6)$$

$$C_G(\rho) = S(\rho_{diag}) - S(\rho) \quad (7)$$

The local coherence only accounts for the coherence in the electron pair system while the global coherence is

the measure of the electron-nuclear coherence. Therefore, in Eq. 6,  $\rho^{el}$  is the density matrix of the electrons that is obtained after partial trace of  $\rho(t)$  (obtained from Eq. 4) over the nuclear spin subspace.  $\rho_{diag}^{el}$  is the density matrix of the electron pair without the off-diagonal terms. In Eq 7,  $\rho$  is the density matrix of the combined (electrons + nuclei) system, and  $\rho_{diag}$  is the combined system's density matrix without the off-diagonal terms. We also use a quantifier called the total coherence measure defined in [3] that captures the coherence summed over the entire evolution period. It is given as:

$$M_i(\rho) = \int_0^\infty C_i(\rho(t)) dt \quad (8)$$

Here  $i \in \{L, G\}$ , corresponds to the local and global coherence respectively.

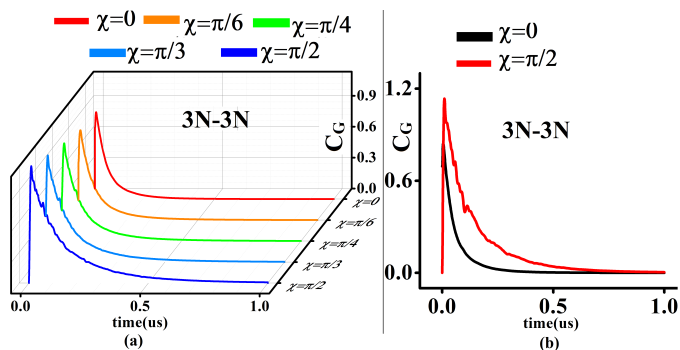


FIG. 2. (a) Relative entropy of global coherence  $C_G$  at  $(k_F, k_R) = (10^6, 10^8) s^{-1}$  for five distinct values of  $\chi$  corresponding to varying degree of spin selectivity due to CISS ( $0, \frac{\pi}{6}, \frac{\pi}{4}, \frac{\pi}{3}, \frac{\pi}{2}$ ). (b) Relative entropy of global coherence  $C_G$  at  $(k_F, k_R) = (10^6, 10^8) s^{-1}$  for two extreme cases  $\chi (0, \frac{\pi}{2})$  showing an increase in coherence time. The calculations have been done for a six nuclei cryptochrome based radical pair system.

In Fig. 2, we have plotted the relative entropy of global coherence  $C_G(\rho)$  with respect to time at  $\theta = 0$  and  $\phi = 0$ . In Fig. 2.(a), we have considered five distinct value of  $\chi$  showing varying degree of spin selectivity due to CISS ( $0, \frac{\pi}{6}, \frac{\pi}{4}, \frac{\pi}{3}, \frac{\pi}{2}$ ). For analysis, we have considered a realistic rate combination  $(k_F, k_R) = (10^6, 10^8) s^{-1}$  for 6-nuclei cryptochrome based molecule. In Fig. 2.(b) we have considered two extreme cases  $\chi = (0, \frac{\pi}{2})$  highlighting the increase in global coherence (magnitude and time duration). A finite value of  $C_G$  for a longer duration of time was observed when  $\chi = \frac{\pi}{2}$  compared to  $\chi = 0$ .

In Fig. 3, we have plotted the relative entropy of local coherence  $C_L(\rho)$  with respect to time. In Fig. 3.(a), we have considered five distinct value of  $\chi = (0, \frac{\pi}{6}, \frac{\pi}{4}, \frac{\pi}{3}, \frac{\pi}{2})$  for a realistic rate combination of  $(k_F, k_R) = (10^6, 10^8) s^{-1}$  for 6-nuclei cryptochrome molecule based radical pair system. In Fig. 3. (b), we have considered two extreme cases i.e.  $\chi = (0, \frac{\pi}{2})$  highlighting the increment in local coherence with CISS. At  $t = 0$ , we observe

the maximum value of  $C_L$  at  $\chi = 0$ . As the spin selectivity increases,  $C_L$  decreases at  $t = 0$ . It can be attributed to the initial value of  $\rho$  at  $t = 0$  i.e. as  $\chi$  increases, the non-diagonal terms of density matrix ( $\rho$ ) associated with radical pair local coherence decrease. However, even though at  $t = 0$ , the system is showing maximum local coherence ( $C_L$ ) at  $\chi = 0$ , the case of full CISS  $\chi = \frac{\pi}{2}$  shows us the sustained coherence over evolution. Hence, we deduce that the radical pair system has sustained coherence due to CISS.

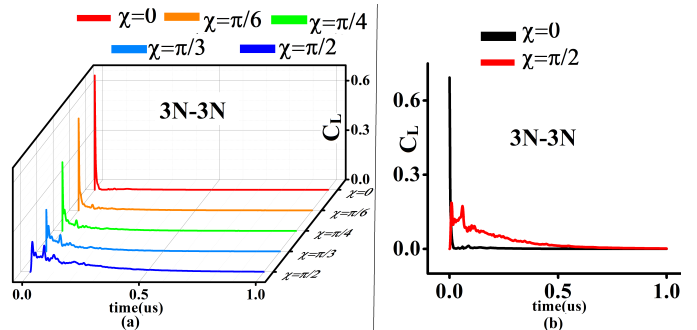


FIG. 3. (a) Relative entropy of local coherence  $C_L$  at  $(k_F, k_R) = (10^6, 10^8) s^{-1}$  for five distinct value of  $\chi$  showing varying degree of spin selectivity due to CISS ( $0, \frac{\pi}{6}, \frac{\pi}{4}, \frac{\pi}{3}, \frac{\pi}{2}$ ). The calculations have been done for six-nuclei cryptochrome based radical pair system. (b) Relative entropy of local coherence  $C_L$  at  $(k_F, k_R) = (10^6, 10^8) s^{-1}$  for two extreme cases i.e.  $\chi = (0, \frac{\pi}{2})$  exhibiting sustained coherence.

In our investigation from Fig. 2 and Fig. 3, it was observed that an increase in CISS results in an increase in coherence. We further confirm this by making use of Eq. 8 that captures the coherence over entire duration of the spin evolution. We plot  $M_i$  as function of spin selectivity  $\chi$  in Fig. 4 at realistic rates of  $(k_F, k_R) = (10^6, 10^8) s^{-1}$  for 2-nuclei (black), 4-nuclei (red), and 6-nuclei (blue) cryptochrome based radical pair system.

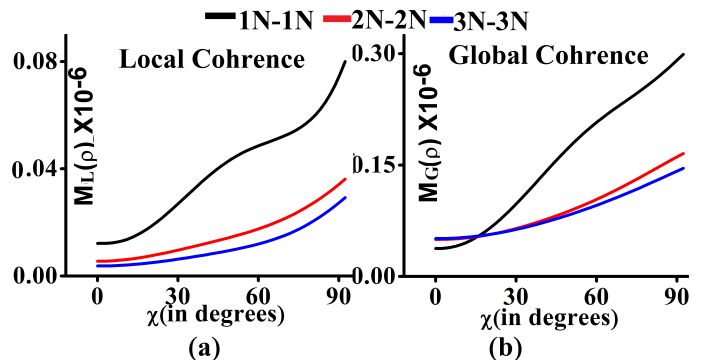


FIG. 4. Relative Entropy of (a) local coherence ( $M_L$ ) and (b) global coherence ( $M_G$ ) at  $(k_F, k_R) = (10^6, 10^8) s^{-1}$  for  $\chi \in [0, \frac{\pi}{2}]$ . This has been done for 2-nuclei (Black), 4-nuclei (Red), and 6-nuclei (Blue) cryptochrome based radical pair system.

As is clear from Fig. 4, the total coherence  $M_i$  ( $i \in$

TABLE I.  $\Delta M_i$  for radical pair model based on 2, 4, and 6 nuclei from cryptochrome based radical pair system for rates  $(k_F, k_R) = (10^6, 10^8) s^{-1}$ .

Nuclei System	$\Delta M_G$	$\Delta M_L$
1N-1N (2-nuclei)	7.97	6.59
2N-2N (4-nuclei)	3.33	6.57
3N-3N (6-nuclei)	2.86	7.82

$\{L, G\}$ ) increases with the degree of CISS. As expected, with the inclusion of more nuclei total coherence of the system decreases for a fixed value of  $\chi$ . To better analyze this, we define another quantity called  $\Delta M_i$  in Eq.9 to quantify the change in total coherence  $M_i$  due to CISS.

$$\Delta M_i = \frac{\max_{\chi \in \{0^\circ, 90^\circ\}}(M_i)}{\min_{\chi \in \{0^\circ, 90^\circ\}}(M_i)} \quad (9)$$

Table I gives the value of  $\Delta M_i$  for all three systems. We observe that all values are greater than unity, signifying an increase in coherence in all systems. However, the value of  $\Delta M_G$  decreases as the number of nuclei increases. The above analysis though performed for  $\theta = 0$  and  $\phi = 0$ , the increase in coherence due to CISS was observed at all orientation of radical with respect to earth's magnetic field.

### B. Effect of Dipolar Interaction

This subsection studies the effect of spin dipolar interaction along with CISS on coherence in the radical pair system. Dipolar interaction ( $D$ ) is governed by Eq. 10 where  $r$  is the distance between two electrons [29].

$$D(r) = -\frac{3 \mu_o \gamma_e^2 \hbar^2}{2 4\pi r^3} \Rightarrow D(r)/\mu T = -\frac{2.78 \times 10^3}{(r/nm)^3} \quad (10)$$

We plot Fig. 5 to study the effect of dipolar interaction on total global and local coherence measures ( $M_G$  and  $M_L$ ). We plot  $M_G$  (Fig. 5. a) and  $M_L$  (Fig.5.b) with respect to  $\chi$ . We plot for five distinct values of dipolar interaction, assuming there is no exchange interaction for the six nuclei from cryptochrome molecule. We take the realistic set of rates  $((k_F, k_R) = (10^6, 10^8) s^{-1})$  in our analysis.

From both plots in Fig.5, we observe that the increase in global coherence due to CISS ( $\Delta M_G$ ) remains constant and is unaffected due to dipolar interaction. However,  $\Delta M_L$  is affected by dipolar interaction and decreases about 13% as  $D$  increases from 0 to 0.4mT. It is summarized and confirmed in Table II. In Fig. 5. (a), we observe that for intermediate values of  $\chi$ , having dipolar interaction increases the total global coherence. To analyze this further, we need to define a quantity called  $\Delta G_{D=i}(\chi)$  and  $\Delta L_{D=i}(\chi)$  given in Eq. 11 and Eq. 12 respectively.  $\Delta G_{D=i}(\chi)$  and  $(\Delta L_{D=i}(\chi))$  compute the difference of total global (local) coherence when  $D = 0$  and when  $D = i$

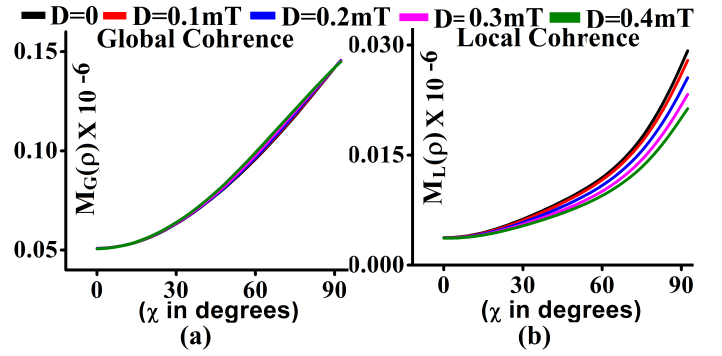


FIG. 5. Relative entropy of (a) global coherence and (b) local coherence at  $(k_F, k_R) = (10^6, 10^8) s^{-1}$  for  $\chi \in [0, \frac{\pi}{2}]$ . A total of five values of  $D$  were assumed (0, 0.1mT, 0.2mT, 0.3mT, and 0.4mT). The exchange interaction was assumed negligible here. The calculations have been done for six nuclei from cryptochrome molecule at  $\theta = 0$  and  $\phi = 0$ .

TABLE II.  $\Delta M_i$  for radical pair model based on six nuclei from cryptochrome molecule for rates  $(k_F, k_R) = (10^6, 10^8) s^{-1}$ .

Dipolar Interaction	$\Delta M_G$	$\Delta M_L$
D=0	2.86	7.82
D=0.1mT	2.86	7.50
D=0.2mT	2.86	6.90
D=0.3mT	2.86	6.31
D=0.4mT	2.86	5.81

where  $i \in \{0.1mT, 0.2mT, 0.3mT, 0.4mT\}$  at a particular  $\chi$ .

$$\Delta G_{D=i}(\chi) = M_{G,D=0}(\chi) - M_{G,D=i}(\chi) \quad (11)$$

$$\Delta L_{D=i}(\chi) = M_{L,D=0}(\chi) - M_{L,D=i}(\chi) \quad (12)$$

In Fig. 6, we plot  $\Delta G_{D=i}$  and  $\Delta L_{D=i}$  as function of  $\chi$ . A horizontal reference line in Fig. 6 depicts  $\Delta G_{D=i} = 0$  and  $\Delta L_{D=i} = 0$ . Anything above this line shows that total coherence is greater when  $D = 0$  than  $D = i$ . Fig. 6. (a) plots  $\Delta G_{D=i}$  where for intermediate values of  $\chi$  we observe a negative value of  $\Delta G_{D=i}$ . It signifies that dipolar interaction enhances global coherence for these values of  $\chi$ . The range of values of  $\chi$  for which we observe an increase in coherence is approximately the same for all values of  $D$ . Fig. 6.(b) discusses  $\Delta L_{D=i}$  where we observe that  $\Delta L_{D=i}$  is always positive for all values of  $D$ . Hence for all values of dipolar interactions, local coherence shows degradation in total local coherence  $M_L$ . The exchange interaction ( $J$ ) further increases total global coherence which is discussed in detail in Appendix A.

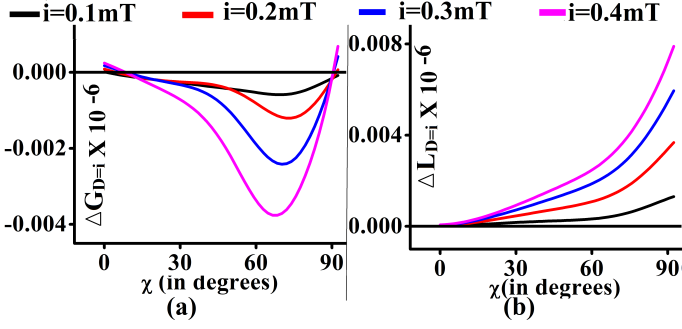


FIG. 6. (a)  $\Delta G_{D=i}$  (b)  $\Delta L_{D=i}$  where  $i$  is 0.1mT (black), 0.2mT (red), 0.3mT (blue), 0.4mT (pink) at  $(k_F, k_R) = (10^6, 10^8) s^{-1}$  for  $\chi \in [0, \frac{\pi}{2}]$ . The horizontal dotted line is the reference line depicting when  $\Delta G_{D=i} = 0$  and  $\Delta L_{D=i} = 0$ . Anything above this line shows that total coherence is greater for the case when  $D = 0$  than when  $D = i$ . This has been done for six nuclei from cryptochrome molecules at  $\theta = 0$  and  $\phi = 0$ .

TABLE III.  $\Delta M_G$  for global coherence for radical pair model based on six nuclei from cryptochrome molecule for various rate combination at  $D = 0$  and  $J = 0$ .

$k_R \downarrow, k_F \rightarrow$	$10^4 s^{-1}$	$10^5 s^{-1}$	$10^6 s^{-1}$	$10^7 s^{-1}$	$10^8 s^{-1}$
$10^4 s^{-1}$	0.98	0.87	0.86	0.84	0.68
$10^5 s^{-1}$	1.57	0.98	0.86	0.84	0.68
$10^6 s^{-1}$	2.44	1.57	0.98	0.86	0.68
$10^7 s^{-1}$	2.78	2.50	1.61	0.99	0.71
$10^8 s^{-1}$	3.82	3.74	2.86	2.01	0.98

### C. Coherence in RP System for Various Rates

In this subsection, we ascertain the increase in coherence with CISS at different rates. We present Tab III and Tab IV that show an increase in total coherence due to CISS (through  $\Delta M_G$  and  $\Delta M_L$ ) for a wide range of rate combinations. We found that maximum value of  $\Delta M_G$  is at  $(k_F, k_R) = (10^4, 10^8) s^{-1}$  and  $\Delta M_L$  is at  $(k_F, k_R) = (10^4, 10^6) s^{-1}$  (maxima occurs at a different rate combination). However, interestingly a lower  $k_F$  (protonation rate) is key to achieve maximum increase in coherence due to CISS.

TABLE IV.  $\Delta M_L$  for local coherence for radical pair model based on six nuclei from cryptochrome molecule for various rate combination at  $D = 0$  and  $J = 0$ .

$k_R \downarrow, k_F \rightarrow$	$10^4 s^{-1}$	$10^5 s^{-1}$	$10^6 s^{-1}$	$10^7 s^{-1}$	$10^8 s^{-1}$
$10^4 s^{-1}$	4.53	2.83	2.52	1.51	0.33
$10^5 s^{-1}$	13.76	4.52	2.66	1.52	0.33
$10^6 s^{-1}$	19.49	13.33	4.13	1.58	0.33
$10^7 s^{-1}$	18.56	16.98	10.04	2.10	0.33
$10^8 s^{-1}$	9.10	8.82	7.82	2.88	0.37

TABLE V.  $\Delta M_i$  for radical pair model based on six nuclei from cryptochrome molecule for various relaxation rate at  $D = 0$  and  $J = 0$   $(k_F, k_R) = (10^6, 10^8) s^{-1}$

Relaxation rate k	$\Delta M_G$	$\Delta M_L$
$k = 0 s^{-1}$	2.86	7.82
$k = 10^4 s^{-1}$	2.78	7.50
$k = 10^5 s^{-1}$	2.76	7.40
$k = 10^6 s^{-1}$	2.67	6.44
$k = 10^7 s^{-1}$	2.32	2.93

## IV. EFFECT OF ENVIRONMENTAL DECOHERENCE

In this section, we take into consideration the decoherence effect of the surrounding system. We modify Eq. 4 to add spin decoherence operators in the Lindblad formalism.

$$\begin{aligned} \frac{d\hat{\rho}}{dt} &= -(Coherent + Recombination. + Decoherence) \\ &= -i[\hat{H}, \hat{\rho}(t)] - \frac{1}{2}k_R[P_R, \hat{\rho}(t)] - k_F\hat{\rho}(t) \\ &\quad + k \sum_n \frac{1}{2} \{2C_n \hat{\rho}(t) C_n^\dagger - \hat{\rho}(t) C_n^\dagger C_n - C_n^\dagger C_n \hat{\rho}(t)\} \end{aligned} \quad (13)$$

In Eq. 13, *Decoherence* corresponds to the spin decoherence occurring due to surrounding environment. Mathematically we take six decoherence operators:  $C_1 = \sigma_x \otimes I_{E2} \otimes I_N$ ,  $C_2 = \sigma_y \otimes I_{E2} \otimes I_N$ ,  $C_3 = \sigma_z \otimes I_{E2} \otimes I_N$ ,  $C_4 = I_{E1} \otimes \sigma_x \otimes I_N$ ,  $C_5 = I_{E1} \otimes \sigma_y \otimes I_N$  and  $C_6 = I_{E1} \otimes \sigma_z \otimes I_N$ .  $I_{E1}$  correspond to the mixed state of electron on FAD radical while  $I_{E2}$  correspond to the mixed state of electron on TrpH radical.  $I_N$  is the combined mixed state of the nuclei and  $k$  is the decoherence rate.

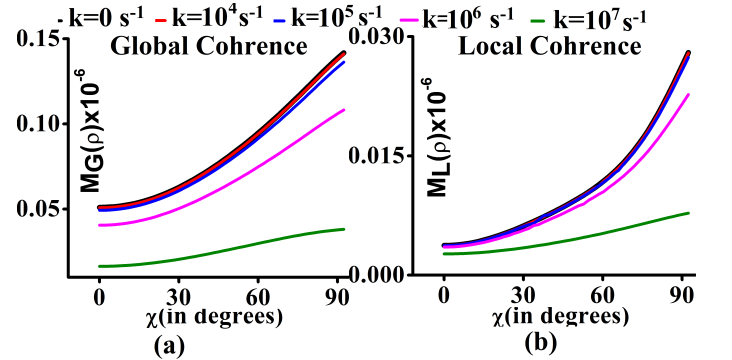


FIG. 7. (a)  $M_G(\chi)$ , (b)  $M_L(\chi)$  where  $k$  is the decoherence rate  $k = 0 s^{-1}$  (black),  $k = 10^4 s^{-1}$  (red),  $k = 10^5 s^{-1}$  (blue),  $k = 10^6 s^{-1}$  (pink) and  $k = 10^7 s^{-1}$  (green). The calculations have been done for six-nuclei cryptochrome based RP system. We have assumed  $D = 0$  and  $J = 0$  here.

In Fig. 7, we plot total global ( $M_G$ ) and local coherence ( $M_L$ ). This calculation has been done at  $(k_F, k_R) =$



$(10^6, 10^8) s^{-1}$  and  $J = 0$  and  $D = 0$ . We observe that at full CISS, coherence is maximum even under decoherence. We have also listed  $\Delta M_G$  and  $\Delta M_L$  with various decoherence rates  $k$  in Tab. V. We observe a reduction in value of  $\Delta M_G$  and  $\Delta M_L$  as decoherence rate  $k$  increases. However, interestingly, we observe increment in coherence due to CISS even at high decoherence rates.

## V. ON UTILITARIAN ROLE OF COHERENCE

In this section, we correlate coherence to the forward product (signalling state) yield of the reaction described in Fig. 1, demonstrating the utilitarian role of coherence. We use the correlation coefficient to show a statistical correlation between signaling state yield and the radical pair spin coherence (both local and global). We use numerous orientations of radical pair with respect to the external magnetic field to show this correlation in a four nuclei system at  $(k_F, k_R) = (10^6, 10^8) s^{-1}$ . The forward (signaling state) yield is defined as:

$$\phi_F = k_F \int_0^\infty P_S(t) dt = k_F \int_0^\infty Tr[\rho(t)] dt \quad (14)$$

Where  $\rho(t)$  is the solution of the master equation Eq. 4,  $Tr$  is the trace over the state density matrix  $\rho$ .  $k_F$  is the rate associated with the signaling state.

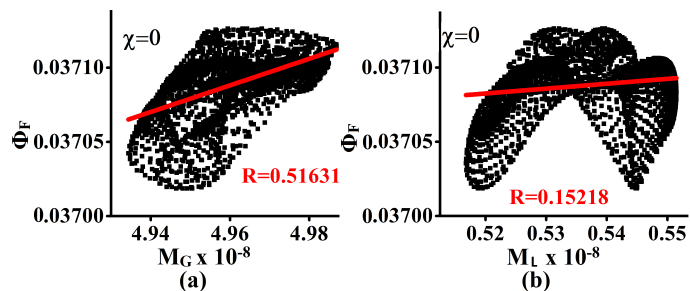


FIG. 8. (a)  $M_G$  vs  $\phi_F$ , and (b)  $M_L$  vs  $\phi_F$  for various values of  $\theta$  and  $\phi$  for  $\chi = 0$ . The calculation is done for four-nuclei from cryptochrome based RP system at  $(k_F, k_R) = (10^6, 10^8) s^{-1}$  with  $D = 0$  and  $J = 0$ . The red line corresponds to the linear fit, and  $R$  (red) corresponds to the correlation coefficient between the coherence measure and signaling state yield.

In Fig. 8.(a), we have plotted the total global coherence ( $M_G$ ) and the signaling state yield ( $\phi_F$ ) for 2500 combinations of  $\theta$  and  $\phi$ . We have taken the values where  $\theta \in \{0^\circ, 180^\circ\}$  and  $\phi \in \{0^\circ, 360^\circ\}$ . The calculation is performed for no CISS case i.e.  $\chi = 0$ . Similarly, in Fig. 8.(b), we have plotted total local coherence ( $M_L$ ) and signaling state yield ( $\phi_F$ ). The  $R$  value (red font) corresponds to the correlation coefficient between the coherence measure and signaling state yield. The red line is the linear fit line corresponding to the scattered points. Similar plots have been plotted for intermediate CISS case (i.e.  $\chi = \frac{\pi}{4}$ ) in Fig. 9 and full CISS case (i.e.  $\chi = \frac{\pi}{2}$ ) in Fig. 10.

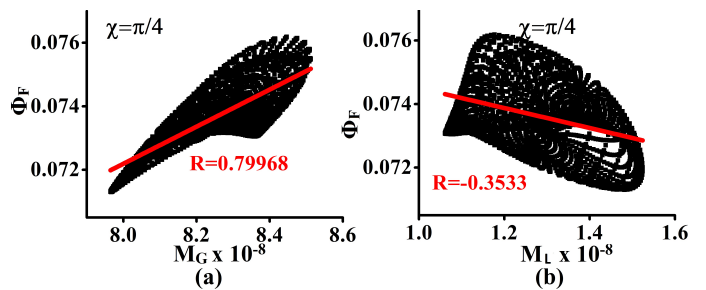


FIG. 9. (a)  $M_G$  vs  $\phi_F$ , and (b)  $M_L$  vs  $\phi_F$  for various values of  $\theta$  and  $\phi$  for  $\chi = \frac{\pi}{4}$ . The calculation is performed for four-nuclei cryptochrome based RP system at  $(k_F, k_R) = (10^6, 10^8) s^{-1}$  with  $D = 0$  and  $J = 0$ . The red line corresponds to the linear fit, and  $R$  (red) corresponds to the correlation coefficient between the coherence measure and signaling state yield.

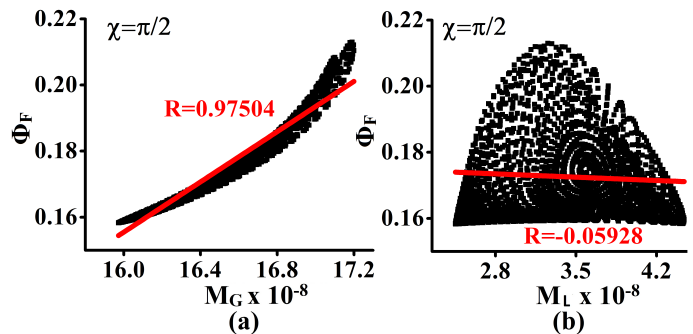


FIG. 10. (a)  $M_G$  vs  $\phi_F$  and (b)  $M_L$  vs  $\phi_F$  for various values of  $\theta$  and  $\phi$  for  $\chi = \frac{\pi}{2}$ . The calculation is performed for four-nuclei from cryptochrome based RP system at  $(k_F, k_R) = (10^6, 10^8) s^{-1}$  with  $D = 0$  and  $J = 0$ . The red line corresponds to the linear fit, and  $R$  (red) corresponds to the correlation coefficient between the coherence measure and signaling state yield.

The total local coherence ( $M_L$ ) has no clear correlation with the signaling state yield ( $\phi_F$ ) for three values of  $\chi$ . Total global coherence ( $M_G$ ) shows a high correlation with the yield of the forward signaling state i.e. as the degree of CISS increases, the correlation parameter  $R$  between total global coherence and signaling state yield increases. In the full CISS case, the value is near unity showing a high correlation of global coherence with the forward signaling state. This forward signaling state is responsible for sending signals to neurons or brains. Hence, global coherence exhibit strong utilitarian role for the compass action than the local coherence i.e. a higher spin selectivity due to chirality leads to a higher correlation of global coherence with forward signaling state yield.

## VI. CONCLUSION

In conclusion, chiral-induced spin selectivity (CISS) effect causes sustained coherence in the radical pair mechanism of avian magnetoreception. It hints towards the possibility that spin coherence might be sustained in a realistic system despite many nuclei for significant time. Moreover, we also observe that the global coherence in the CISS-assisted avian compass is strongly correlated with the signaling state yield. This indicates that unlike local coherence, global coherence has strong utilitarian role in the compass action. We also observe that dipolar and exchange interactions are generally detrimental to the coherence of the avian compass, but their effect can be countered by CISS. All these conclusions confirm the significance of CISS in the avian compass spin dynamics.

## ACKNOWLEDGMENTS

This work is supported by the Science and Engineering Research Board, Department of Science and Technology (DST), India with grant No. CRG/2021/007060 and DST/INSPIRE/04/2018/000023. The authors would also like to thank Department of Electronics and Communication, IIT Roorkee and Ministry of Education, Government of India for supporting Y.T.'s graduate research.

### Appendix A: Effect of Exchange Interaction

In order to understand the role of exchange interaction in six nuclei-based cryptochrome systems, we assume a fixed value of dipolar interaction of  $D = 0.4mT$ . We consider four values of exchange interaction which are less than dipolar interaction ( $J = 0, J = 0.1mT, J = 0.2mT, J = 0.3mT$ ) [29].

In Fig.11, we have plotted  $M_G$  and  $M_L$  for four distinct values of exchange interaction at  $D = 0.4mT$  for six nuclei from cryptochrome. We take the realistic set of rates ( $(k_F, k_R) = (10^6, 10^8)s^{-1}$ ) in our analysis. Corresponding to Fig.11.(a),(b) we have summarized in Table VI the increase in total global(  $\Delta M_G$ ) and local coherence(  $\Delta M_L$ ) due to CISS. We observe that  $\Delta M_G$  and  $\Delta M_L$  first increase and then decreases with exchange interaction. To analyze the effect of exchange interaction for intermediate cases of CISS, we define a quantity as follows.

$$\Delta G_{J=i}(\chi) = M_{G,J=0}(\chi) - M_{G,J=i}(\chi) \quad (A1)$$

$$\Delta L_{J=i}(\chi) = M_{L,J=0}(\chi) - M_{L,J=i}(\chi) \quad (A2)$$

According to Eq. A1,  $\Delta G_{J=i}(\chi)$  compute the difference of total global coherence when their is  $J = 0$  and when  $J = i$  where  $i \in \{0.1mT, 0.2mT, 0.3mT\}$  at a particular  $\chi$ . A similar quantity is defined for total local

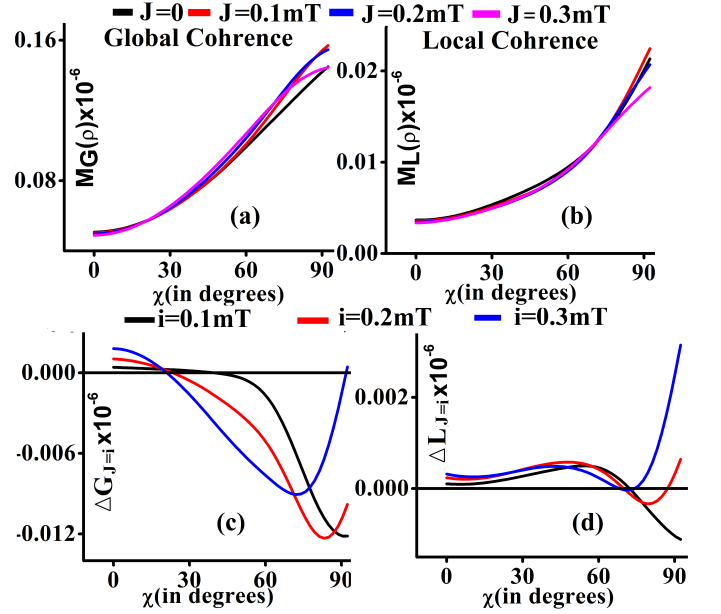


FIG. 11. Relative Entropy of (a) global Coherence and (b) local Coherence at  $(k_F, k_R) = (10^6, 10^8)s^{-1}$  for  $\chi \in [0, \frac{\pi}{2}]$ . A total of four values of  $J$  was assumed (0, 0.1mT, 0.2mT, 0.3mT). (c)  $\Delta G_{J=i}$  (d)  $\Delta L_{J=i}$  where  $i$  is 0.1mT (black), 0.2mT (red), 0.3mT (blue) at  $(k_F, k_R) = (10^6, 10^8)s^{-1}$ . The horizontal dotted line is the reference line depicting when  $\Delta G_{J=i} = 0$  and  $\Delta L_{J=i} = 0$ . A value above this depicts total coherence under no exchange interaction ( $J = 0$ ) having a value greater than when  $J = i$ . The analysis has been done for  $D = 0.4mT$ . This has been done for six nuclei from a cryptochrome molecule at  $\theta = 0$  and  $\phi = 0$ .

TABLE VI.  $\Delta M_i$  for radical pair model based on 6 nuclei from cryptochrome molecule for rate at  $D = 0.4mT$ ,  $(k_F, k_R) = (10^6, 10^8)s^{-1}$ .

Dipolar Interaction	$\Delta M_G$	$\Delta M_L$
J=0	2.86	5.81
J=0.1mT	3.12	6.29
J=0.2mT	3.11	6.03
J=0.3mT	2.95	5.42

coherence  $\Delta L_{J=i}(\chi)$  in Eq. A2. In Fig. 11(c),(d), we plot the  $\Delta G_{J=i}(\chi)$  and  $\Delta L_{J=i}(\chi)$  for a fixed value of  $D = 0.4mT$ . A reference horizontal line is drawn depicting  $\Delta G_{J=i} = 0$  and  $\Delta L_{J=i} = 0$ . Anything above this line depicts that total coherence is greater for the case when  $J = 0$  compared to when  $J$  has finite value  $i$ .

Fig. 11.(c) discuss the difference in  $\Delta G_{J=i}$  where we observe that for intermediate value of  $\chi$ , we obtain a negative value. Exchange interaction further enhances global coherence for these values of  $\chi$ . The window of values of  $\chi$  for which we observe an increase in coherence increases with exchange being maximum for  $J = 0.3mT$ . The increase in coherence is, however, maximum for case  $J = 0.1mT$ . Fig. 11.(d) discuss the difference in  $\Delta L_{J=i}$  where we observe that for certain  $\chi$ , we get a negative

value. The window of values of  $\chi$  for which we observe an increase in local coherence decrease with exchange being maximum for  $J = 0.1mT$ . That means for these values of  $\chi$ , exchange interaction enhances local coherence.

Hence we observe that for intermediate cases of CISS, total coherence shows an improvement when dipolar and exchange interaction affects the radical pair.

- 
- [1] J. Cai and M. B. Plenio, Chemical compass model for avian magnetoreception as a quantum coherent device, *Physical review letters* **111**, 230503 (2013).
- [2] I. Kominis, Quantum relative entropy shows singlet-triplet coherence is a resource in the radical-pair mechanism of biological magnetic sensing, *Physical Review Research* **2**, 023206 (2020).
- [3] R. Jain, V. S. Poonia, K. Saha, D. Saha, and S. Ganguly, The avian compass can be sensitive even without sustained electron spin coherence, *Proceedings of the Royal Society A* **477**, 20200778 (2021).
- [4] E. M. Gauger, E. Rieper, J. J. Morton, S. C. Benjamin, and V. Vedral, Sustained quantum coherence and entanglement in the avian compass, *Physical review letters* **106**, 040503 (2011).
- [5] T. Ritz, S. Adem, and K. Schulten, A model for photoreceptor-based magnetoreception in birds, *Biophysical journal* **78**, 707 (2000).
- [6] P. J. Hore and H. Mouritsen, The radical-pair mechanism of magnetoreception, *Annual review of biophysics* **45** (2016).
- [7] L. D. Smith, J. Deviers, and D. R. Kattnig, Observations about utilitarian coherence in the avian compass, *Scientific reports* **12**, 1 (2022).
- [8] L. D. Smith, F. T. Chowdhury, I. Peasgood, N. Dawkins, and D. R. Kattnig, Driven radical motion enhances cryptochrome magnetoreception: Toward live quantum sensing, *The Journal of Physical Chemistry Letters* **13**, 10500 (2022).
- [9] H. Hiscock, *Long-lived spin coherence in radical pair compass magnetoreception*, Ph.D. thesis, University of Oxford (2018).
- [10] H. G. Hiscock, S. Worster, D. R. Kattnig, C. Steers, Y. Jin, D. E. Manolopoulos, H. Mouritsen, and P. Hore, The quantum needle of the avian magnetic compass, *Proceedings of the National Academy of Sciences* **113**, 4634 (2016).
- [11] C. T. Rodgers and P. J. Hore, Chemical magnetoreception in birds: the radical pair mechanism, *Proceedings of the National Academy of Sciences* **106**, 353 (2009).
- [12] S. Dalum and P. Hedegård, Theory of chiral induced spin selectivity, *Nano letters* **19**, 5253 (2019).
- [13] K. Michaeli and R. Naaman, Origin of spin-dependent tunneling through chiral molecules, *The Journal of Physical Chemistry C* **123**, 17043 (2019).
- [14] S. Matityahu, Y. Utsumi, A. Aharony, O. Entin-Wohlman, and C. A. Balseiro, Spin-dependent transport through a chiral molecule in the presence of spin-orbit interaction and nonunitary effects, *Physical Review B* **93**, 075407 (2016).
- [15] B. Göhler, V. Hamelbeck, T. Markus, M. Kettner, G. Hanne, Z. Vager, R. Naaman, and H. Zacharias, Spin selectivity in electron transmission through self-assembled monolayers of double-stranded dna, *Science* **331**, 894 (2011).
- [16] R. Naaman and D. H. Waldeck, Chiral-induced spin selectivity effect, *The journal of physical chemistry letters* **3**, 2178 (2012).
- [17] R. Naaman and D. H. Waldeck, Spintronics and chirality: Spin selectivity in electron transport through chiral molecules, *Annu. Rev. Phys. Chem* **66**, 263 (2015).
- [18] J. Xu, L. E. Jarocho, T. Zollitsch, M. Konowalczyk, K. B. Henbest, S. Richert, M. J. Golesworthy, J. Schmidt, V. Déjean, D. J. Soward, *et al.*, Magnetic sensitivity of cryptochrome 4 from a migratory songbird, *Nature* **594**, 535 (2021).
- [19] S. Y. Wong, Y. Wei, H. Mouritsen, I. A. Solov'yov, and P. Hore, Cryptochrome magnetoreception: four tryptophans could be better than three, *Journal of the Royal Society Interface* **18**, 20210601 (2021).
- [20] T. P. Fay, Chirality-induced spin coherence in electron transfer reactions, *The Journal of Physical Chemistry Letters* **12**, 1407 (2021).
- [21] J. Luo and P. Hore, Chiral-induced spin selectivity in the formation and recombination of radical pairs: cryptochrome magnetoreception and epr detection, *New Journal of Physics* **23**, 043032 (2021).
- [22] T. Baumgratz, M. Cramer, and M. B. Plenio, Quantifying coherence, *Physical review letters* **113**, 140401 (2014).
- [23] A. Streltsov, G. Adesso, and M. B. Plenio, Colloquium: Quantum coherence as a resource, *Reviews of Modern Physics* **89**, 041003 (2017).
- [24] A. Winter and D. Yang, Operational resource theory of coherence, *Physical review letters* **116**, 120404 (2016).
- [25] G. Katsoprinakis, A. Dellis, and I. Kominis, Coherent triplet excitation suppresses the heading error of the avian compass, *New Journal of Physics* **12**, 085016 (2010).
- [26] Y. Tiwari and V. S. Poonia, Role of ciss in the radical pair model of avian magnetoreception (2022).
- [27] F. Cintolesi, T. Ritz, C. Kay, C. Timmel, and P. Hore, Anisotropic recombination of an immobilized photoinduced radical pair in a 50- $\mu$ t magnetic field: a model avian photomagnetoreceptor, *Chemical Physics* **294**, 385 (2003).
- [28] T. P. Fay, L. P. Lindoy, D. E. Manolopoulos, and P. Hore, How quantum is radical pair magnetoreception?, *Faraday discussions* **221**, 77 (2020).
- [29] O. Efimova and P. Hore, Role of exchange and dipolar interactions in the radical pair model of the avian magnetic compass, *Biophysical Journal* **94**, 1565 (2008).